

# Analytical Method for Evaluating the Quality of Acoustic Fields Radiated by a Multielement Therapeutic Array with Electronic Focus Steering

S. A. Ilyin<sup>a</sup>, P. V. Yuldashev<sup>a</sup>, V. A. Khokhlova<sup>a</sup>, L. R. Gavrilov<sup>b</sup>,  
P. B. Rosnitskiy<sup>a</sup>, and O. A. Sapozhnikov<sup>a</sup>

<sup>a</sup>Moscow State University, Moscow, 119991 Russia

<sup>b</sup>Andreev Acoustical Institute, ul. Shvernika 4, Moscow, 117036 Russia

e-mail: sergey\_ilyin@acs366.phys.msu.ru; gavrilov@akin.ru

Received June 19, 2014

**Abstract**—The paper presents an analytical method for calculating and analyzing the quality of 3-D acoustic fields of multielement phased arrays used in noninvasive ultrasound surgical devices. An analytical solution for the far field of each of its elements is used when calculating the array field. This method significantly accelerates calculations while preserving the high accuracy of results as compared to conventional direct numerical integration. Radiation from typical phased arrays is calculated using this approach, and the quality of their dynamic focusing is analyzed. Undesired diffraction effects caused by electronic focus steering are considered: an amplitude decrease in the main maximum and the appearance of grating lobes. The quality of dynamic focusing of the acoustic fields of two practically interesting arrays with a quasi-random element distribution (256 and 1024 elements, respectively), as well as of the regular array consisting of 256 elements is compared. In addition as well, a study is made of how the dimensions of the array elements and their spatial distributions affect the dimensions of the areas in which dynamic focusing is possible without occurrence of strong grating lobes and significant decrease in pressure amplitude at the main focus.

**Keywords:** medical acoustics, ultrasound surgery, focusing, diffraction, multielement therapeutic arrays, electronic focus steering

**DOI:** 10.1134/S1063771015010042

## INTRODUCTION

Ultrasound focusing radiators are widely used in modern medical applications to perform noninvasive (without direct intervention) surgical operations [1–3]. Recently, high-power multielement phased arrays have come into use for this technology, making it possible to independently vary the amplitudes and phases of elements, to electronically steer the focus, and to create different combinations of several foci [4].

Multielement phased arrays typically consist of a large number of relatively small-sized elements, each of which is an individual piezoelectric transducer (Fig. 1). Different methods are applied to calculate ultrasound fields depending on the structure of the array and the shape of its elements. The majority of them are based on application of the Rayleigh integral [5] and its numerical implementation. Various methods are used to calculate the entire array field quickly and efficiently. For example, in [4], the field from an individual array element was calculated numerically, stored, and further used to calculate the total contribution from all array elements using geometrical conversion of the spatial coordinates (turns and shifts)

taking into account the position of the elements. With such an approach, it is necessary to calculate the field parameters of an individual element in nodes of a 3-D rectangular mesh. However, after subsequent turning and shifting of this mesh, its nodes do not coincide with the nodes of the main coordinate mesh; therefore interpolation becomes necessary. As a result, a certain loss of accuracy occurs. At the same time, this method is quite fast. To further accelerate calculations, the method was recently implemented on a computer with graphics processors [6]. In the case when the near field of the transducer is of interest, special simplifications have been proposed to eliminate singularity when calculating the Rayleigh integral near the surface of the transducer [7, 8].

This work proposes a method of calculating the fields of multielement arrays with flat circular elements as a combination of analytic solutions for the Rayleigh integral in the far field of each of the elements [9]. Several standard multielement arrays were used as examples to demonstrate the possibility of applying this method to quickly and accurately calculate their fields in a volume, as well as to further analyze the quality of such fields.

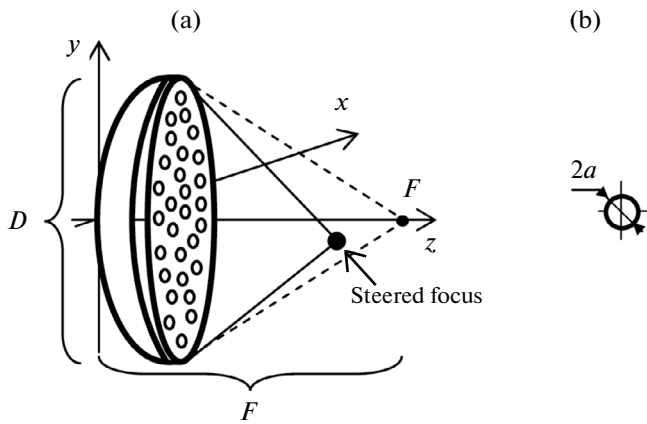


**Fig. 1.** General diagram of multielement phased array. (a) Side view of array, (b) sketch of array element.  $D$ , array diameter;  $F$ , radius of curvature of array surface;  $a$ , radius of array element.

One of the major properties of multielement arrays is the possibility of electronic steering of their foci. When considering this property, it is necessary to take into account the undesirable side effects caused by the discrete structure of the arrays. In particular, these effects include the decrease in the field amplitude in the main focus and the appearance of grating lobes [4]. As suggested earlier [4, 10–12], the degree of manifestation of these effects is used here as a quality criterion for the field generated by a given array. To evaluate side effects, it is necessary to measure or numerically calculate the 3-D fields for different locations of the electronically steered array focus, which is a time-consuming process. Therefore, large steps are commonly used for steering the focus, and the field is analyzed only in the steering plane, i.e., in the plane containing the array axis and the focus itself. With such an approach, there is the probability of missing the

hotspot lying between the nodes of the calculation mesh or outside the plane of the focus steering.

The analytic method used in this work makes it possible to calculate the fields of multielement phased arrays much faster than by direct numerical integration, while preserving the accuracy of the results. In addition, it enables analyzing fields generated by arrays in an entire volume and with a small step of the focus steering.

As an example of applying the method, we analyzed the quality of fields generated by two phased arrays with quasi-random distributions of their elements [4] and one phased array with a regular distribution. The quasi-random arrays consisted of 256 and 1024 elements and the regular array consisted of 256 elements. The array with 256 randomly positioned elements (Fig. 1) corresponded to an ultrasound source in the experimental setup at Imperial College London [4]; it had the following parameters: diameter  $D = 170$  mm, surface curvature radius  $F = 130$  mm, element radius  $a = 3.5$  mm, operating frequency  $f = 1.0$  MHz. The regular array with 256 elements had the same parameters and differed only in the distribution of the elements. The array with 1024 elements had the same radiation area as the array with 256 elements; accordingly, the element radius was two times smaller,  $a = 1.75$  mm, while the frequency, diameter, and surface curvature radius were the same. The packing density of the elements on the surfaces of all the arrays was 52% for the active part with a size of 160 mm without taking into account the surface curvature. Therefore, for the same intensity at the elements, the radiating acoustic power was the same for all three arrays. Figure 2 schematically shows spatial distributions of the elements of these arrays. Using the analytic approach, we studied focusing in water, calculated the curves of nearly continuous focus steering, and analyzed the quality of the generated fields in a volume. By considering the array with 1024 elements, we also

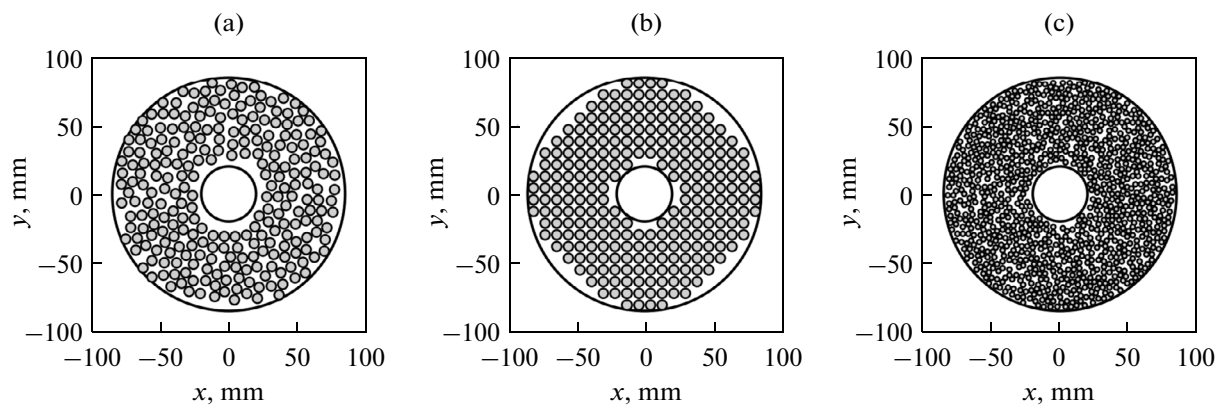


**Fig. 2.** Spatial distributions of elements for different types of arrays considered in this paper, view along array axis. (a) Array with quasi-random distribution of 256 elements with radius of  $a = 3.5$  mm, (b) array with regular distribution of 256 elements of same size, (c) array with quasi-random distribution of 1024 elements with radius of  $a = 1.75$  mm.

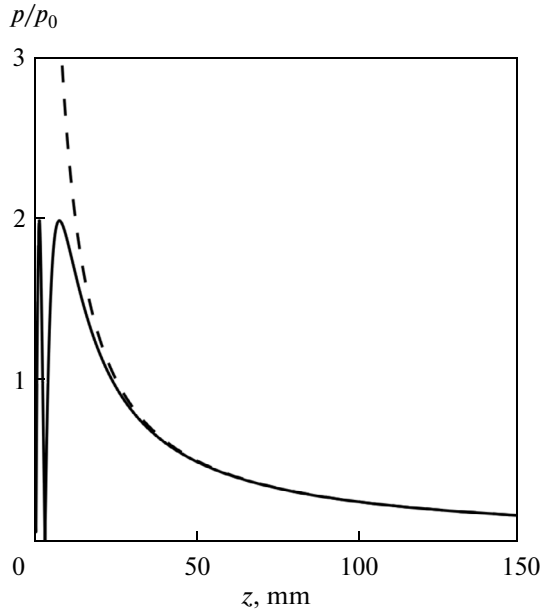


**Fig. 3.** Comparison of pressure amplitude distributions along axis of single element of array with radius of  $a = 3.5$  mm: exact analytic solution on axis (solid line) and analytic solution in far field of element (dashed line).

studied how an increase in the number of elements affects the quality of the generated field.

### THEORETICAL MODEL

Figure 1 shows a general diagram of a typical multielement array used in noninvasive surgery. The array comprises a spherical cup with round piston elements the normals to which are directed at the geometrical center of the array's curvature [4]. The phase of each element of the array can be varied independently. The origin of the coordinate system was chosen as the center of the array, and axis  $z$  was directed along its axis. To electronically steer the focus, the initial phase for each of the array elements was set taking into account the delay in the time of flight from the center of an element to the generated focus (Fig. 1).

In the linear formulation, the radiating field of the entire array is the sum of the acoustic fields radiating from each of its elements. The acoustic pressure of the  $j$ th element in complex form can be calculated using the Rayleigh integral [5]:

$$p_j(\mathbf{r}, t) = -\frac{i\omega\rho_0 e^{-i\omega t}}{2\pi} \int_{S_j} \frac{v_n(\mathbf{r}') e^{ikR}}{R} dS', \quad (1)$$

where  $i$  is the imaginary unit,  $\omega = 2\pi f$  is the angular frequency of the radiator,  $k = \omega/c_0$  is the wavenumber,  $c_0$  is the sound velocity,  $\rho_0$  is the density of the medium,  $S_j$  is the surface area of an element,  $v_n$  is the complex amplitude of the normal component of the vibration velocity at the surface of the transducer, and

$R$  is the distance from the surface element  $dS'$  to the observation point.

In conventional approaches, integral (1) is calculated numerically, which requires division of the surface of the transducer into quite small elements (much smaller than the wavelength); because of this, calculation in the general case takes a long time. To avoid this difficulty, it is possible to take into account the specific features of the array sources. For therapeutic treatments, the region near the geometrical focus is of interest and thus, the distance to the focus from each of the array elements is much larger than the length of its near field:  $F \gg z_R$ , where  $z_R = ka^2/2$ . Therefore, already at relatively small distances from the array surface, the observation point can be considered located in the far field diffraction region of an element. It is well known that for the majority of transducers with simple geometry, the pressure distribution in their far field region can be calculated analytically [5]. This means that the entire field of the array can also be calculated analytically by summing the solutions of the far fields of individual elements. Such an analytic approach had not been applied previously for calculating the acoustic fields of multielement therapeutic arrays.

Let us consider a multielement array consisting of flat circular elements and assume that the normal component of the vibration velocity is constant along the surface of each element (piston source). The analytic solution for the complex amplitude of acoustic pressure in the far field of such an element is known [5]:

$$p(\theta, r) = -\frac{ip_0 z_R e^{ikr}}{r} \frac{2J_1(ka \sin \theta)}{ka \sin \theta}, \quad (2)$$

where  $p_0 = \rho_0 c_0 v_n$  is the characteristic pressure at the surface of the element,  $r$  is the distance from the center of the element to the observation point,  $\theta$  is the angle between the element axis and a ray from the center of the element to the observation point, and  $J_1$  is the first-order Bessel function.

To determine the limits of applicability of the far field approximation for an array element, we compared the solution (2) to the known exact analytic solution for the field of a flat circular element along its axis [5]:

$$\frac{p(\theta = 0, r = z)}{p_0} = -2i \exp \left[ i \frac{k}{2} (\sqrt{a^2 + z^2} + z) \right] \times \sin \left[ \frac{k}{2} (\sqrt{a^2 + z^2} - z) \right]. \quad (3)$$

Here,  $z$  is the coordinate along the element axis.

As one can see from Fig. 3, beginning already from the distances of  $z = 35$  mm from the center of an array element ( $z_R = 26$  mm), the analytic solution is almost indistinguishable from the exact solution, the difference being a tenth of a percent. Thus, the overall field

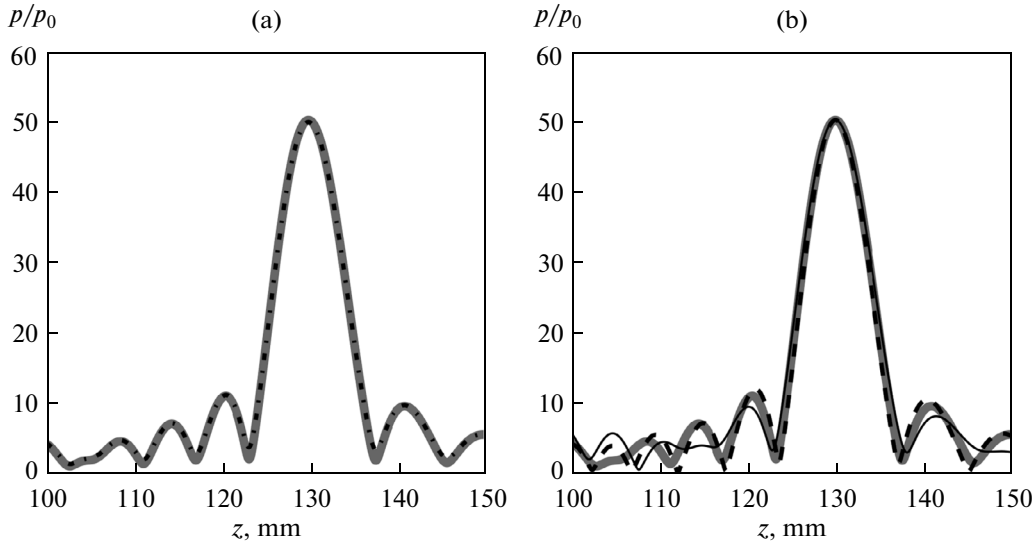


**Fig. 4.** Pressure amplitude distributions along axis  $z$  of array. (a) Comparison of analytic solution (thick gray line) and numerical calculation of Rayleigh integral (black dash-dotted line) for array with quasi-random distribution of 256 elements. (b) Comparison of analytic solution for array with random distribution of 256 elements (thick gray line), array with regular distribution of 256 elements (solid black line), and array with quasi-random distribution of 1024 elements (dashed black line).

of the array at larger distances can be calculated by summing the solutions for each element:

$$p(\mathbf{r}) = \sum_j p_j(\theta_j, r_j), \quad (4)$$

where  $p_j$  is the pressure contribution from the  $j$ th array element and  $(\theta_j, r_j)$  are the cylindrical coordinates in the local coordinate system with respect to the indicated element.

This new calculation method was compared to the conventional approach based on taking the Rayleigh integral numerically. The entire array field was calculated by the following equation obtained after replacing integral (1) by the corresponding summation over small integration elements of the area  $S_j$ :

$$p(\mathbf{r}) = -\frac{ikp_0}{2\pi} \sum_{S_j} \frac{e^{ikR_j}}{R_j} S_j. \quad (5)$$

Here,  $R_j$  is the distance from the center of each integration element  $S_j$  of the entire surface of the array to the observation point. In our calculations, we divided the tangent plane into triangles as was done in [13].

Spatial distributions of the array field were calculated in water (sound velocity  $c_0 = 1500$  m/s, density  $\rho_0 = 1000$  kg/m<sup>3</sup>) on a grid in a Cartesian coordinate system with the grid step and a focus steering step of 0.1 mm. The accuracy and, therefore, the duration of numerical calculations using the Eq. (5) depended on the number of integration elements into which the surface of the array was divided. For instance, when the active surface of the array was divided into 4188 elements (this choice ensured a calculation error of less than 0.1%), calculation of a 3-D field with dimensions of  $100 \times 100 \times 100$  points (volume  $10.0 \times 10.0 \times$

$10.0$  mm, step 0.1 mm) took around 20 min for a personal computer (Intel Core 2 Duo, dual cores, 2.0 GHz, 4 GB RAM), whereas when using the proposed analytic approach, this time was around 3 s. If the quality of the array field is analyzed when steering the focus in a set of points ( $100 \times 100 \times 100$  points) and calculating the Rayleigh integral numerically for each point, it will take more than a week for the same computer, which is unachievable in practice. When the analytic approach is applied, the same calculation takes less than 24 hours, which is faster by more than an order of magnitude. This makes it possible to use the method to develop specialized software for studying acoustic fields of multielement arrays in real time [14].

## RESULTS

To check the accuracy of the results obtained by the analytic method (4) for the entire array field, we compared them to the solutions obtained by direct numerical calculation (5). Figure 4a shows the pressure amplitude distributions along the axis  $z$  of the array with 256 randomly distributed elements, calculated analytically and numerically. One can see from the figure that at distances  $z > 100$  mm, the analytic solution already almost coincides with the numerical one.

Figure 4b shows the pressure amplitude distributions that were analytically calculated along the axis  $z$  for the arrays with 256 randomly and regularly distributed elements, as well as for the random array with 1024 elements. As one can see, in the region close to the focus ( $z = 130$  mm) that includes up to three diffraction lobes of the arrays, the distributions are very

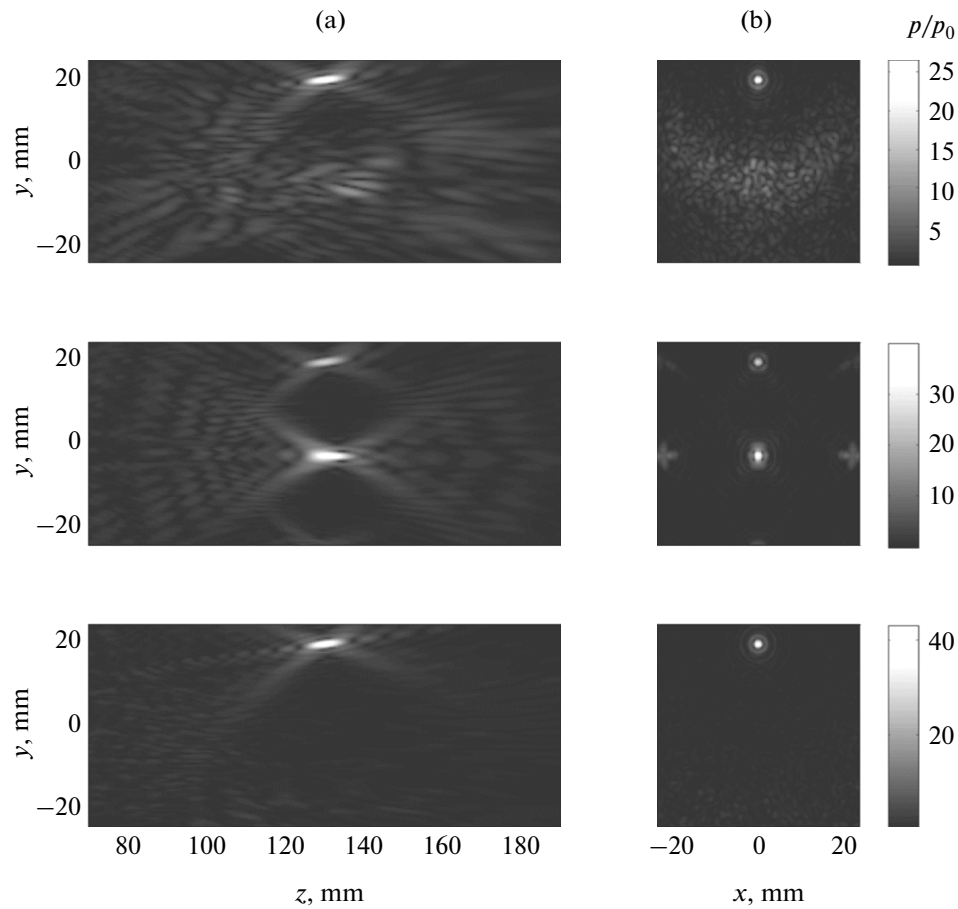


**Fig. 5.** Two-dimensional pressure amplitude distributions when steering focus by 20 mm from array axis ( $x = 0$ ,  $y = 20$  mm,  $z = 130$  mm) for different types of arrays. (a) Distributions in plane along array axis, (b) distributions in plane perpendicular to array axis and passing through the center of its curvature. Top row, array with quasi-random distribution of 256 elements; middle row, array with regular distribution of 256 elements; bottom row, array with quasi-random distribution of 1024 elements.

close to each other both in shape and in pressure amplitude for all the arrays considered. Certain differences in the distributions are observed closer to the transducer and farther beyond from the focus; they are related to differences in the positioning of the array elements and their dimensions.

When the focus is shifted from the center of curvature of the array ( $x = 0$ ,  $y = 0$ ,  $z = 130$  mm), side effects related to the discrete structure of the array begin to manifest themselves. Figure 5 shows the 2-D pressure amplitude distributions in the plane of the focus steering  $yz$  (Fig. 5a) and in the plane  $xy$  perpendicular to the axis  $z$  and passing through the center of curvature of the array surface (Fig. 5b). The distributions were obtained for the 20 mm shift of the focus along the coordinate  $y$  from the array axis. For illustrative purposes, these and subsequent distributions were calculated for the pressure amplitude but not for the ultrasound intensity, which is quadratically proportional to the pressure. One can see that when the focus is shifted, the field structures of the considered arrays show significant differences. For example, for the

array with 256 randomly distributed elements (Fig. 5, top row), the pressure amplitude in the main maximum decreases by approximately 60% in comparison to the case without steering (Fig. 4); at the same time, a region of discrete scattered grating lobes is formed in the lower parts of the pattern. The largest pressure amplitude in the grating lobe for such an array in this case is 35% of the amplitude at the focus. The increase in the number of randomly distributed array elements and corresponding decrease in their radius lead to much less pressure amplitude level of the grating lobes (up to 1% of the amplitude at the focus), they are virtually unseen on the distribution, and the pressure in the main maximum is larger (up to 85% in comparison to the case without focus steering) (Fig. 5, bottom row). For the array with regular distribution of 256 elements (Fig. 5, middle row), formation of one grating lobe is observed, the pressure level in which even exceeds the pressure level in the main focus by 15%. These results agree with the data obtained previously in [4].

An increase in the number of array elements (and a corresponding decrease in their dimensions) leads to significant broadening of the operational region of the focus steering both from the viewpoint of the occurrence of grating lobes and from the viewpoint of the decreasing pressure amplitude in the main maximum. A random positioning of elements on the array surface additionally broadens the region of a safe focus steering without the occurrence of strong grating lobes.

Figure 6 illustrates the effects of a decrease in pressure amplitude in the main maximum and the occurrence of grating lobes for a gradual focus steering in the plane  $yz$  for the considered arrays. The pressure amplitude levels were analyzed in the entire volume of the field of the array. In the figure, thin contours represent the regions of the focus steering within the limits when the main pressure maximum decreases by 10, 30, and 50% of the maximum achievable value. Since the decrease in pressure amplitude during the focus steering is determined by the directivity pattern of each array element, which depends on their size, for both arrays with 256 elements of identical size ( $a = 3.5$  mm), the regions of the decrease in pressure in the main maximum virtually coincide (Figs. 6a and 6b). For the array with 1024 elements two times smaller in size ( $a = 1.75$  mm), the linear dimension of these regions in the transverse direction is approximately twice larger. For two arrays with larger size elements, characteristic dimensions of the region of the half-level of the intensity maximum (0.7 of the pressure maximum) are identical: 23 mm in cross section and 60 mm along the axis; for the array with elements of smaller size, 42 and 87 mm, respectively.

Thick contours in Fig. 6c also show regions of focus steering in which the intensity of the largest grating lobe does not exceed 10% of the intensity (32% of the pressure amplitude) in the main maximum, which is the accepted criterion of a safe irradiation [4, 10–12]. Thus, for the arrays with randomly distributed elements of smaller size ( $a = 1.75$  mm), the region of a safe focus steering without the occurrence of strong grating lobes substantially exceeded the region of the decreasing pressure amplitude in the main maximum to a level of 0.5. Meanwhile, for the array with 256 randomly distributed larger elements ( $a = 3.5$  mm), the region of a safe focus steering is located between the contours of the decreasing pressure amplitude at the focus with levels of 0.7 and 0.5 (Fig. 6). For the regular array of 256 elements ( $a = 3.5$  mm, Fig. 6b), there is practically no region of a safe focus steering.

Thus, one can see that a regular array of 256 elements is completely unacceptable for practical application due to the appearance of grating lobes of large amplitude already with the minimum focus steering. When steering the focus of the random array with 256 elements, the safe working zone is the region of the half-decrease in intensity (0.7 of the pressure level) in the main maximum, since the region that satisfies the safety criterion on the pressure amplitude level of

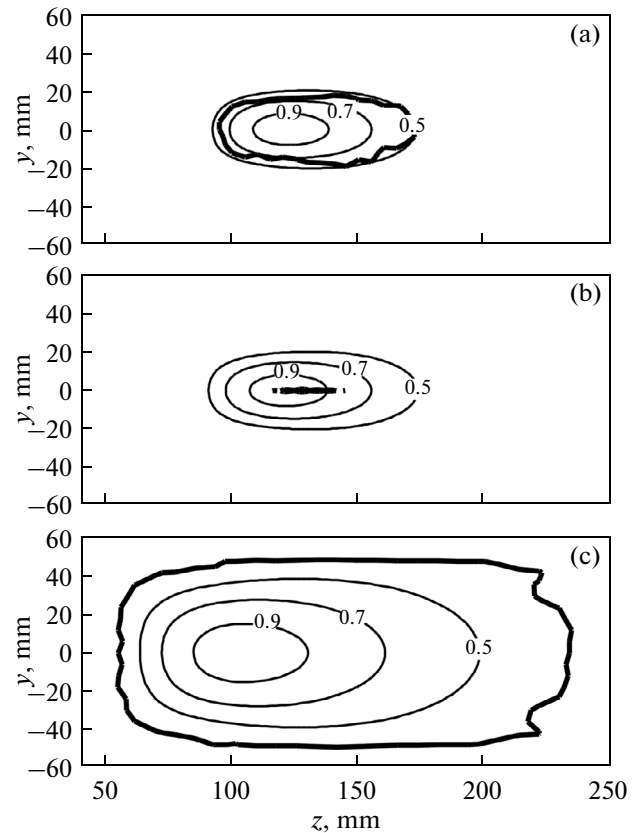


**Fig. 6.** Contours of focus steering corresponding to decrease in pressure amplitude in main maximum by 10, 30, and 50% of largest achievable value (thin curves) and contours where intensity of the grating lobes reaches 10% of intensity in main maximum (thick line). (a) Results for array with quasi-random distribution of 256 elements, (b) for array with regular distribution of 256 elements, (c) for array with quasi-random distribution of 1024 elements.

grating lobes is much larger. When using an array with a larger number of elements (1024) of smaller size, the safety criterion for the level of grating lobes can be neglected; the region of their occurrence exceeds even the region of the decrease in intensity in the main focus by a factor of 4 (0.5 of the pressure level). This agrees with the results obtained previously in [4].

Although it is intuitively clear that the arrays with a large number of elements have an acoustic field structure such that the grating lobes will occur in the plane of the focus steering, this problem has not yet been studied. The proposed analytic method has made it possible to quickly analyze the acoustic field structure in the entire volume (Fig. 6). Calculations have shown that for the arrays considered here, the grating lobes are actually located either in the plane of the focus steering or at a distance less than 2 mm from it. However, in some cases, the grating lobes were found at distances of up to 8 mm from the plane of the focus steering. Nevertheless, these cases were not of practical interest, since the focus was positioned within the

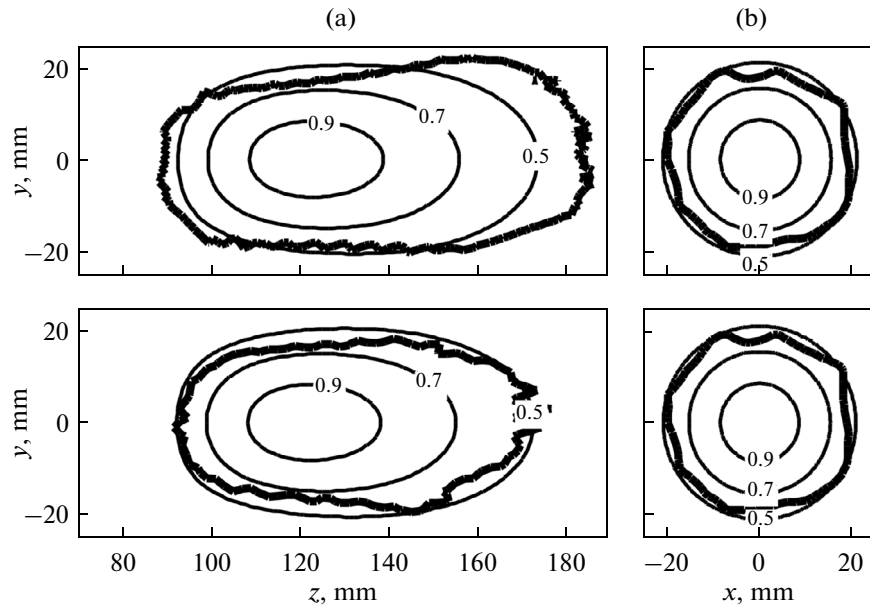


**Fig. 7.** Contours of focus steering corresponding to decrease in pressure amplitude in main maximum by 10, 30, and 50% of largest achievable value (thin lines) and contours where intensity of grating lobes reaches 10% of intensity in the main maximum (thick lines) for array with quasi-random distribution of 256 elements. Top half, search for grating lobes only in plane of focus steering; bottom half, search for grating lobes in entire volume. (a) Plane along array axis, (b) plane perpendicular to array axis and passing through its center of curvature.

region where the pressure amplitude in the main maximum was already more than two times smaller than its maximum achievable value. When it is necessary to steer the focus to such a point, a mechanical positioner is usually employed, which moves the array itself and its focus as it is realized in the clinical Philips Sonalleve MR-HIFU system [15].

Figure 7 shows the differences when searching for grating lobes only in the plane of the focus steering (upper half) and in the volume (lower half) using as an example the obtained regions of the safe focus steering of the random array with 256 elements (thick curves). One can see that the differences are not very strong, but noticeable enough to be taken them into account when accurate results are needed.

## CONCLUSIONS

This paper illustrates the application of an analytic method for fast analysis of the quality of fields generated by powerful ultrasound arrays with a dynamic steering of their foci. The key feature of the method is the use of an analytic solution for the far field of each of the array elements, which makes it possible to analyze fields of multielement arrays in the entire volume and with small steps in focus steering. Such an approach can accelerate calculations by more than two orders of magnitude in comparison to direct numerical calculation of the Rayleigh integral.

As an example, the quality of fields generated by different types of arrays with steering of their foci was

compared. The field quality criteria chosen here were the criteria of the decrease in acoustic field intensity in the main maximum up to a certain level and the level of the occurring grating lobes (<10% of the intensity in the main maximum), both of which have been adopted in the literature.

It was demonstrated that there were differences in determining the safe regions of focus steering when searching for grating lobes only in the plane of the focus steering or in the entire volume of the array field. Although in some cases considered here, the grating lobes occurred at a certain distance from the focus steering plane, in practically interesting cases they were located in this plane.

The proposed algorithm enables fast analysis of fields generated by arrays of different configurations and with different dimensions of elements. In the case of arrays with larger elements and less symmetry, as well as when generating multifocal configurations [16], the effect of the occurrence of grating lobes outside the plane of the focus steering can be more pronounced. In this case, the proposed rapid calculation method is irreplaceable when searching for dangerous grating lobes in the entire volume. It is also of interest to extend the method for describing fields of arrays whose elements have different shapes, e.g., square, for which an analytic solution in the far field also exists.

## ACKNOWLEDGMENTS

The work was supported by the Russian Science Foundation grant no. 14-12-00974.

## REFERENCES

1. *Physical Principles of Medical Ultrasonics*, Ed. by K. Hill, J. Bember, and G. Khaar (Wiley, Chichester, 2004; Fizmatlit, Moscow, 2008).
2. M. R. Bailey, V. A. Khokhlova, O. A. Sapozhnikov, S. G. Kargl, and L. A. Crum, *Acoust. Phys.* **49**, 369 (2003).
3. L. R. Gavrilov, *Focused Ultrasound of High Intensity in Medicine* (Fazis, Moscow, 2013) [in Russian].
4. L. R. Gavrilov and J. W. Hand, *IEEE Trans. Ultrason. Ferroelectr. Freq. Contr.* **47**, 125 (2000).
5. H. T. O'Neil, *J. Acoust. Soc. Am.* **21**, 516 (1949).
6. M. Hlawitschka, R. J. McGough, K. W. Ferrara, and D. E. Kruse, *IEEE Trans. Ultrason. Ferroelectr. Freq. Contr.* **58**, 2001 (2011).
7. D. Chen and R. J. McGough, *J. Acoust. Soc. Am.* **124**, 1526 (2008).
8. J. F. Kelly and R. J. McGough, *IEEE Trans. Ultrason. Ferroelectr. Freq. Contr.* **53**, 1150 (2006).
9. S. A. Ilyn, P. V. Yuldashev, V. A. Khokhlova, L. R. Gavrilov, and O. A. Sapozhnikov, *Proc. Sci. Conf. "Sess. Sci. Council of Russ. Acad. Sci. on Acoustics" and 25th Sess. Russ. Acoust. Soc.* (2012), vol. 2, p. 87.
10. S. A. Goss, L. A. Frizell, J. T. Kouzmanoff, J. M. Barich, and J. M. Yang, *IEEE Trans. Ultrason. Ferroelectr. Freq. Contr.* **43**, 1111 (1996).
11. E. S. Ebbini and C. A. Cain, *IEEE Trans. Biomed. Eng.* **38**, 634 (1991).
12. E. B. Hutchinson, M. T. Buchanan, and K. Hynynen, *Med. Phys.* **23**, 767 (1996).
13. P. V. Yuldashev and V. A. Khokhlova, *Acoust. Phys.* **57**, 334 (2011).
14. P. B. Rosnitskiy, S. A. Ilyn, O. A. Sapozhnikov, and V. A. Khokhlova, *Uch. Zapiski Fiz. Fak. Mos. Gos. Univ.* **4**, 134301-1 (2013).
15. W. Kreider, P. V. Yuldashev, O. A. Sapozhnikov, N. Farr, A. Partanen, M. R. Bailey, and V. A. Khokhlova, *IEEE Trans. Ultrason. Ferroelectr. Freq. Contr.* **60**, 1683 (2013).
16. L. R. Gavrilov, *Acoust. Phys.* **49**, 508 (2003).

*Translated by A. Carpenter*